Earthquake Magnitude Estimation using Precise Point Positioning

Jakub Nosek [1,2], Pavel Václavovic [2]

[1] Brno University of Technology, Veveri 331/95, Brno, Czech Republic
[2] Geodetic Observatory Pecný, RIGTC, Ustecka 98, Zdiby, Czech Republic

jakub.nosek@pecny.cz

Abstract. An accurate estimation of an earthquake magnitude plays an important role in targeting emergency services towards affected areas. Along with the traditional methods using seismometers, site displacements caused by an earthquake can be monitored by the Global Navigation Satellite Systems (GNSS). GNSS can be used either in real-time for early warning systems or in offline mode for precise monitoring of ground motion. The Precise Point Positioning (PPP) offers an optimal method for such purposes, because data from only one receiver are considered and thus not affected by other potentially not stable stations. Precise external products and empirical models have to be applied, and the initial convergence can be reduced or eliminated by the backward smoothing strategy or integer ambiguity resolution. The product for the magnitude estimation is a peak ground displacement (PGD). PGDs observed at many GNSS stations can be utilized for a robust estimate of an earthquake magnitude. We tested the accuracy of estimated magnitude scaling when using displacement waveforms collected from six selected earthquakes between the years 2016 and 2020 with magnitudes in a range of 7.5–8.2 Moment magnitude M_W. We processed GNSS 1Hz and 5Hz data from 182 stations by the PPP method implemented in the G-Nut/Geb software. The precise satellites orbits and clocks corrections were provided by the Center for Orbit Determination in Europe (CODE). PGDs derived on individual GNSS sites formed the basis for ground motion parameters estimation. We processed the GNSS observations by the combination of the Kalman filter (FLT) and the backward smoother (SMT), which significantly enhanced the kinematic solution. The estimated magnitudes of all the included earthquakes were compared to the reference values released by the U. S. Geological Survey (USGS). The moment magnitude based on SMT was improved by 20% compared to the FLT-only solution. An average difference from the comparison was 0.07 M_W and 0.09 M_W for SMT and FLT solutions, respectively. The corresponding standard deviations were 0.18 M_W and 0.22 M_W for SMT and FLT solutions, which shows a good consistency of our and the reference estimates.

1. Introduction

Earthquakes with a moment magnitude M_W greater than seven often cause extensive damage to buildings and loss of life. Large earthquakes can lead to other devastating phenomena such as tsunamis, landslides, and sometimes volcanic eruptions. Early information on the magnitude of the earthquake is essential for evacuating people and protecting critical infrastructure. Knowledge of the extent of the damage is essential for the government in planning and managing assistance to the affected regions.

Content from this work may be used under the terms of the Creative Commons Attribution 3.0 licence. Any further distribution of this work must maintain attribution to the author(s) and the title of the work, journal citation and DOI.
Published under licence by IOP Publishing Ltd

The main characteristic of an earthquake is its magnitude. The previously used Richter scale has been replaced by the moment magnitude scale M_W [1]. The magnitude moment of the scale indicates a total amount of energy released by an earthquake, and it is not saturated during large earthquakes compared to the Richter scale [2]. Traditional methods for determining the magnitude of earthquakes are based on data from broadband seismometers and strong-motion accelerometers. During large earthquakes, seismometric and accelerometric data may be saturated or clipped. The magnitude estimated from such data is then incorrect.

Global Navigation Satellite Systems (GNSS) data has become an important source for earthquakes detection and monitoring over the last 20 years. First, GNSS have begun to be used for long-term crustal deformation monitoring [3] and later for tsunami early warning systems [4]. The GNSS data publicly available usually have a sampling interval 30 s. Therefore, it can only be used for monitoring permanent displacements caused by earthquakes. The availability of high-rate GNSS observations (sampling rate ≥ 1 Hz) in real-time in recent years has enabled the GNSS data to be included in the earthquake and tsunami early warning systems worldwide.

The input product for determining the magnitude of an earthquake is the so-called peak ground displacement (PGD) extracted from the GNSS coordinates time series. Compared to traditional methods using P-wave measurements, the magnitude determination based on the GNSS PGDs is slower (typically a few seconds to minutes due to the faster propagation of P-waves). On the other hand, GNSS PGDs provide an unsaturated estimate of the magnitude. Several authors have already described the magnitude of scaling using PGDs. Gutenberg [5] introduced an empirical model for magnitude estimation when exploiting the horizontal PGDs. The PGD scaling law introduced by Crowell et al. [6] is based on five earthquakes and uses three-dimensional PGDs. This scaling law has been improved several times. The latest PGDs scaling law coefficients based on data from 29 earthquakes were calculated by Ruhl et al. [7].

Jing and Su used high-rate GNSS PGDs to estimate the magnitude of $M_W = 7.9$ located 280 km south-east of the Kodiak earthquake [8]. They processed 1Hz GNSS data from 78 GNSS stations using Precise Point Positioning (PPP). They estimated the magnitude of the earthquake $M_W = 7.97 \pm 0.18$ with an average deviation of 0.07 M_W from the reference value of the earthquake released by the U. S. Geological Survey (USGS). In a similar study [9], Su and Jin estimated the magnitudes of two earthquakes with an accuracy of 0.3 M_w compared to USGS reference values. Hongcai et al. achieved an average difference of 0.18 M_W between GNSS PGDs derived moment magnitude and moment magnitude derived from seismic data, respectively [10].

While an earthquake magnitude represents an overall character of an earthquake, intensity is a site-dependent parameter with different values in different areas. An observed intensity depends on a magnitude, a distance to the epicenter, a depth of the event, an acceleration of the earth, a period of seismic waves, and the local geological structure. The frequently used Modified Mercalli Intensity Scale (MMI) [11] depends on key responses such as waking people, movement of furniture, damage to chimneys, and finally, destroying buildings. The MMI indicates the danger of the event in Roman numerals from I (not felt shaking) to X (extreme shaking).

A good contribution to intensity maps (e.g. USGS Intensity Map) is, in addition to classic data, also data provided by people within the USGS Community Internet Intensity System using the application "Did You Feel It?" (DYFI) [12]. Currently, people contribute to this system with their earthquake experience in near real-time, making DYFI an interesting product for assessing an extent of earthquake damage. Jing and Su determined a preliminary relationship between seismic intensity and ground motion parameters based on data from 18 selected GNSS stations [8].

Our goal is to determine a preliminary PGD-based intensity model for Alaska on the basis of processing GNSS data from several stations surrounding the epicentres of three earthquakes in 2018 and in 2020 using Precise Point Positioning method. An alternative model will be determined when using publicly available global PGD products provided by the Database of Strong-Motion Displacements [7]. We show that the intensity model is regional dependent, therefore the global one is not precise enough. We also compared results from different GNSS data processing techniques. The achieved earthquake intensity model is evaluated on the basis of comparing with the data from the DYFI service.

2. Data description

Precise product and models such as: precise satellite orbits and clocks, satellite and receiver antenna phase center models, site-specific coefficients of ocean tide loading, and Earth rotation parameters are needed for achieving high accuracy PPP results. In April 2021, the Center for Orbit Determination in Europe (CODE) completed the CODE repro3 solution [13] in order to contribute to the International GNSS Service (IGS) repro3 campaign. The results of this campaign became the best candidate for input products to our processing. CODE repro3 provides consistent precise products for the period 1994–2020, which includes satellite clocks with 5 seconds temporal resolution, which are advantageous for high-rate PPP processing.

We selected 6 earthquakes (M_w 7.5–8.2) from 2016–2020 for our study (Table 1 and Figure 1). We processed GNSS data from two different providers. GNSS data from 3 earthquakes in Alaska (2018, 2x 2020), 1 earthquake in Mexico (2017), and 1 earthquake in Honduras (2018) were obtained from the University Navstar Consortium (UNAVCO). UNAVCO collects various technology data from many contributors (UNAVCO community investigators, http://www.unavco.org). UNAVCO provides low-rate and high-rate GNSS observations and other data from thousands of stations around the world. GNSS data from the New Zealand earthquake (2016) were provided by New Zealand GeoNet network (ftp://ftp.geonet.org.nz). We processed 1 Hz and, if available, 5 Hz GNSS observations in RINEX format version 2.xx from a total of 182 sites.

Table 1. Selected earthquakes dataset.

Event	Country	Origin Time	Number of GNSS Stations
M_W 7.6 - 99 km SE of Sand Point	Alaska (USA)	2020-10-19 20:54:38	34
M_W 7.8 - 99 km SSE of Perryville	Alaska (USA)	2020-07-22 06:12:44	40
M_W 7.9 - 280 km SE of Kodiak	Alaska (USA)	2018-01-23 09:31:41	27
M_W 7.5 - 44 km E of Great Swan Island	Honduras	2018-01-10 02:51:33	21
M_W 8.2 - 101 km SSW of Tres Picos	Mexico	2017-09-08 04:49:19	21
M_W 7.8 - 54 km NNE of Amberley	New Zealand	2016-11-13 11:02:56	39

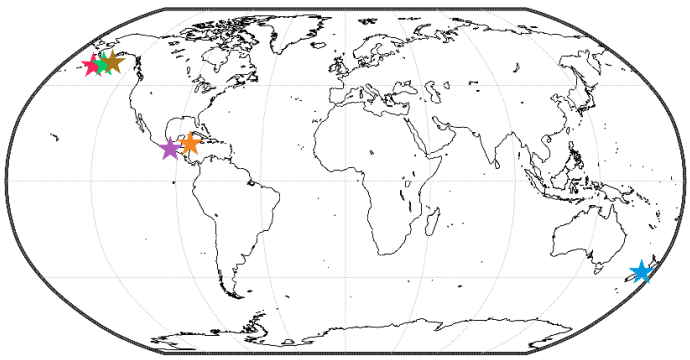

Figure 1. Overview of 6 selected earthquakes.

Earthquake magnitude, origin times, and epicenter location reference values were obtained from the USGS website [14]. Intensity Summaries of DYFI data were obtained from the page of each USGS event at https://earthquake.usgs.gov/.

3. Data processing

We performed the quality control (QC) of all used RINEX observation files with the G-Nut/Anubis software [15]. The QC results revealed the content of observation files such as: available GNSS constellations, satellites, bands/frequencies, observation signals, and also several qualitative characteristics such as: code multipath, phase cycle-slips, receiver clock-jumps, and the number of expected observations.

The lack of observed epochs can significantly worsen the PPP solution. Therefore, we monitored the ratio of existing/expected observations. Stations with an existing/expected ratio of less than 60 % were excluded. Such ratios at selected stations are visualized in Figure 2.

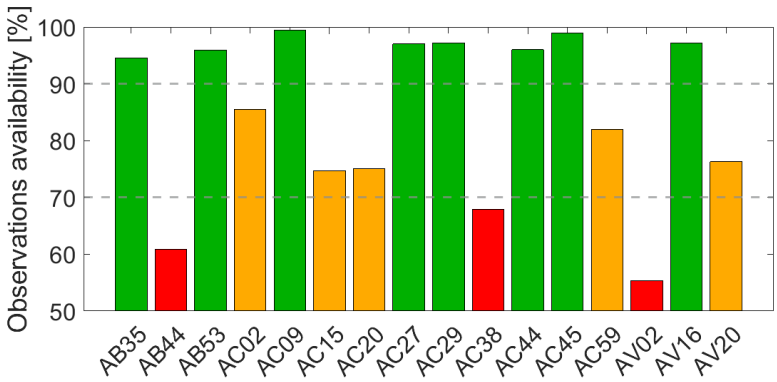

Figure 2. Observations availability at selected stations during M_W 7.9 - 280 km SE of Kodiak earthquake.

We have utilized the Precise Point Positioning (PPP) method for processing collected code and carrier phase observations from GPS and GLONASS satellites. The PPP is based on processing undifferenced observations, therefore data from only one station are included in a solution, which prevents connection to reference stations possibly influenced by a site displacement due to an earthquake. Precise orbits and clocks of all available satellites are then essential input products. Such products were provided by the Center for Orbit Determination in Europe (CODE), which has conducted the third reprocessing campaign when using precise models compliant with the latest standards and thus obtained homogenous, reliable, and consistent solution. We used the Square root forward filter for solving the normal equations, which is a more numerically stable alternative to the traditional Kalman filter. The state vector including all estimated parameters suffer from initial convergence taking usually tens of minutes. The initial convergence and also possible re-convergence can be shorten by integer ambiguity resolution, which requires additional carrier phase hardware biases. Moreover, precise local atmospheric parameters are necessary for further initial convergence reduction. However, the initial convergence can be eliminated efficiently using the backward smoothing algorithm, which can lead to comparable accuracy as that from the integer ambiguity resolution [16]. As a result, we used the RTS backward smoother for improving precision during the whole processing interval and still preserving the high-rate coordinates solution. The processing strategy and used models are summarized in the Table 2.

Table 2. Processing strategy, models, and used precise products.

Item	Parameter
Estimator	Square root filter / RTS backward smoother
Observations	Pseudorange and carrier phase observations
Constellations	GPS + GLONASS
Sampling rate	1 Hz / 5 Hz
Elevation cut-off	7°
Observation weighting	Elevation dependent 1/sin(elevation)^2
Satellite orbits/clocks	CODE repro3 (fixed)
Ionospheric delay	Eliminated using the ionosphere-free combination
Tropospheric delay	Zenith hydrostatic delay: Saastamoinen Zenith wet delay: estimated with 0.5 mm/sqrt(hour) random walk process noise
Receiver clock offset	Estimated as white noise
Phase-windup	Corrected
Attitude of satellites	Nominal models (eclipsed satellites not used)
Antenna phase centers	Corrected with igsR3_2077.atx file
Station displacement	IERS Convention 2010 (solid Earth tides, ocean tide loading, pole tide)
Ambiguity	Float (convergence eliminated by the smoothing)

We transformed the time series of coordinates obtained from PPP from Earth Center Earth Fixed (ECEF) realized in ITRF2014 into the East, North, Up (ENU) local topocentric system. To estimate the magnitude of the earthquake at *i*th GNSS site, we calculated the PGD as

$$\mathrm{PGD}_i = \max\left(\sqrt{\mathrm{E}_i^2 + \mathrm{N}_i^2 + \mathrm{U}_i^2}\right). \quad (1)$$

To prevent PGDs at remote stations from being falsely detected before the arrival of a seismic wave, a travel time mask outward from the source of the earthquake of 3 km/s is applied. According to Crowell et al. [6], the relationship between PGD and M_w can be written as

$$\log \mathrm{PGD} = \mathrm{A} + \mathrm{B} \times M_w + \mathrm{C} \times M_W \times \log D\ , \quad (3)$$

where D is the distance to the hypocenter in kilometers and A, B, C are the regression coefficients. We used scaling law coefficients A = -5.919, B = 1.009, C = -0.145 derived in [7]. M_w can be calculated inversely to (3) as

$$M_{w\,i} = \frac{\log \mathrm{PGD}_i - A}{B + \mathrm{C} \times \log D}\ . \quad (4)$$

Finally, the magnitude estimate of the earthquake is calculated as the average of the magnitude estimates of the individual sites.

According to [17], the relationship between MMI and PGD can be written as

$$\mathrm{MMI} = A + B \times \log \mathrm{PGD}\ , \quad (5)$$

where PGD is in units of centimeters and A, B are the regression coefficients. Firstly, we calculated the global relationship between PGD and intensity on the basis of PGDs from the six selected earthquakes we processed and then when using the PGDs from the Database of Strong-Motion Displacements [7]. In the case of Database of Strong-Motion Displacements, only earthquakes with a magnitude similar to our 6 processed earthquakes were used (M_w 7.4–8.3). PGD-intensity coefficients were calculated using the least squares adjustment. The input values were PGDs and DYFI intensities obtained from USGS. Only PGDs with a distance of less than 20 km closest to the DYFI response were used. The weighting of PGDs / MMI observations depended on the distance between the observed PGDs and the nearest DYFI report and the number of DYFI responses on the site.

To calculate the relationship between PGD and MMI for the Alaska region, we used PGDs from three Alaskan earthquakes (2018, 2× 2020). The processing was the same as for the global dataset.

4. Results

PGDs were extracted from time series of ENU coordinates. We compared the estimated coordinates from the forward filter only (FLT) with the coordinates improved also with the backward smoother (SMT). Such comparison is visible in the Figure 3. A purple vertical line in the image indicates the beginning of the earthquake at 06:12:44 UTC. The SMT solutions are less noisy and more precise, therefore, we used the SMT results for the PGD extraction from time series. All other images presented are based on SMT solutions.

The Figure 4 displays the E (red) and N (blue) displacement components at stations AB13, AC40, AV34, AV08, and AV0 caused by the earthquake with the magnitude Mw = 7.8 and with the epicenter located 99 km SSE of Perryville. The figure shows a decrease in displacement with increasing distance from the epicenter of the earthquake.

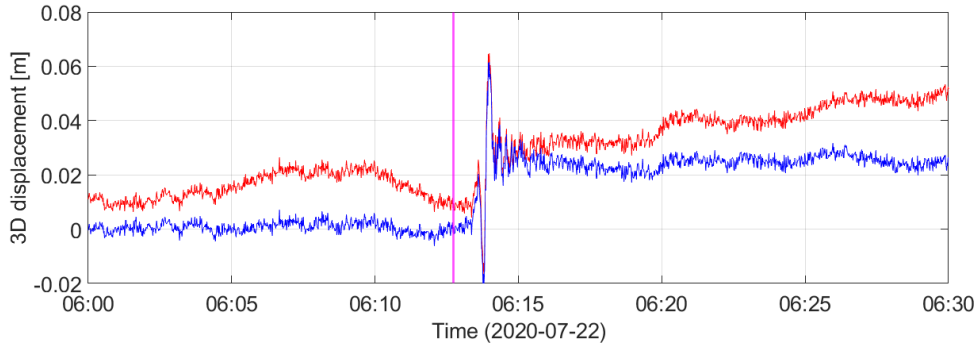

Figure 3. SMT (blue) and FLT (red) displacement waveforms at station AC21 during M_W 7.8 - 99 km SSE of Perryville (Alaska) earthquake. The magenta line shows earthquake origin time.

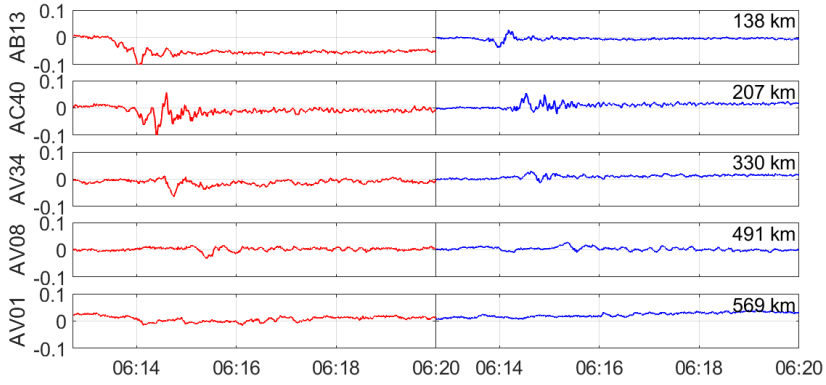

Figure 4. East (red) and North (blue) displacement components at GNSS stations AB13, AC14, AV34 AV08, and AV40 during MW 7.8 - 99 km SSE of Perryville (Alaska) earthquake.

Table 3 shows the resulted characteristics of individual earthquakes. The estimated magnitudes of all the included earthquakes were compared to the reference values released by the USGS. An average difference from the comparison was 0.07 M_W and 0.09 M_W for SMT and FLT solutions, respectively. SMT provides more accurate estimates of magnitude than FLT (mean of RMS_{SMT} = 0.18 M_W, mean of RMS_{FLT} = 0.22 M_W). Backward smoothing, therefore, allows a 20% improvement in the M_W estimate.

Table 3. Statistical results of magnitude calculation.

Event	M_w (FLT)	M_W (SMT)	RMS_{FLT}	RMS_{SMT}	Number of GNSS Stations
M_W 7.6 - 99 km SE of Sand Point	7.68	7.64	0.25	0.23	34
M_W 7.8 - 99 km SSE of Perryville	7.89	7.87	0.23	0.19	40
M_W 7.9 - 280 km SE of Kodiak	7.84	7.84	0.22	0.16	27
M_W 7.5 - 44 km E of Great Swan Island	7.60	7.58	0.19	0.13	21
M_W 8.2 - 101 km SSW of Tres Picos	8.04	8.11	0.24	0.19	21
M_W 7.8 - 54 km NNE of Amberley	7.76	7.86	0.19	0.15	39
Total	–	–	0.22	0.18	182

Differences between the estimated magnitudes at the individual stations and the reference values from the USGS are shown in figure 5. The estimated magnitudes at each station are displayed as red dots. The figures show a small trend in the estimation of size depending on the distance from the epicenter.

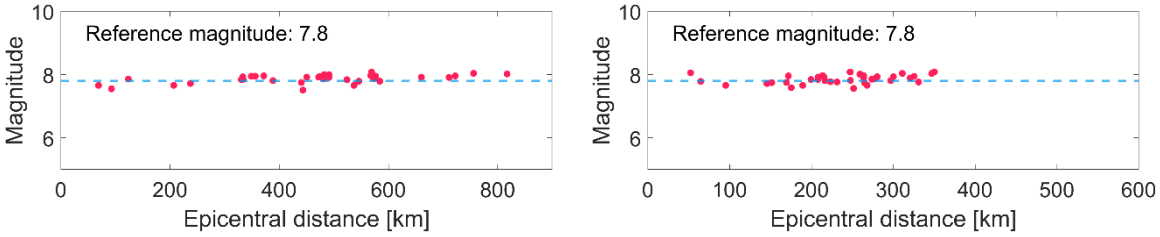

Figure 5. Comparison of reference magnitudes released by USGS (blue line) and magnitudes estimated at individual stations during M_W 7.8 - 99 km SSE of Perryville earthquake (left) and M_W 7.8 - 54 km NNE of Amberley earthquake (right).

The relationship between PGDs and epicentral distance is shown in figure 6. According to equation (3), PGDs are displayed as a function of epicentral distances and magnitudes. The red line represents the estimated magnitude. The blue line represents the reference magnitude (M_W = 7.8).

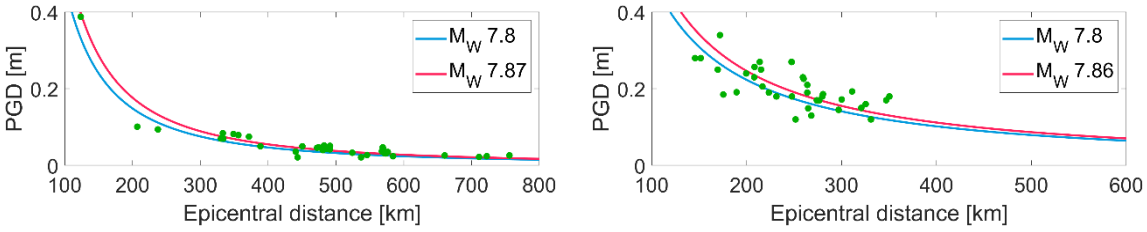

Figure 6. Comparison between PGDs determined at individual stations (green dots) and predicted PGDs according to magnitude values by (3) during M_W 7.8 - 99 km SSE of Perryville earthquake (left) and M_W 7.8 - 54 km NNE of Amberley earthquake (right)

Table 4 shows the estimated coefficients of the relationship between PGD and intensity according to (5). A good consistency can be seen between the global model calculated from our estimated PGD from 6 selected earthquakes and the model calculated from data provided by the Database of Strong-Motion Displacements [7]. However, we can see more significant differences in coefficients between the global and regional (Alaska) models, therefore, the global model is not optimal for regional applications. Figure 7 (left) shows the application of the model to PGDs during M_W 7.8 - 99 km SSE of Perryville earthquake using local model coefficients according to table 4. DYFI response intensity reference values are shown

in Figure 7 (right). It can be seen that the model captures reality relatively well. Figure 8 shows the intensities during the M_W of 7.9 - 280 km SE of the Kodiak earthquake.

Table 4. Coefficients of PGD-intensity models.

Model	A	B
Global (6 selected earthquakes)	3.60	-0.84
Global (Database of Strong-Motion Displacements [7])	3.57	-0.91
Alaska	4.72	-0.69

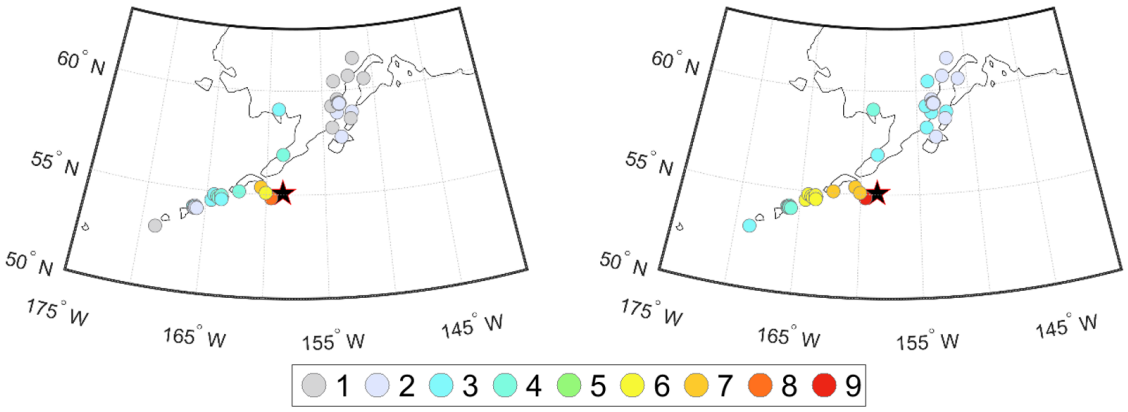

Figure 7. Alaska regionally modeled (left) and DYFI reported (right) macro-intensity values during M_W 7.8 - 99 km SSE of Perryville (Alaska) earthquake.

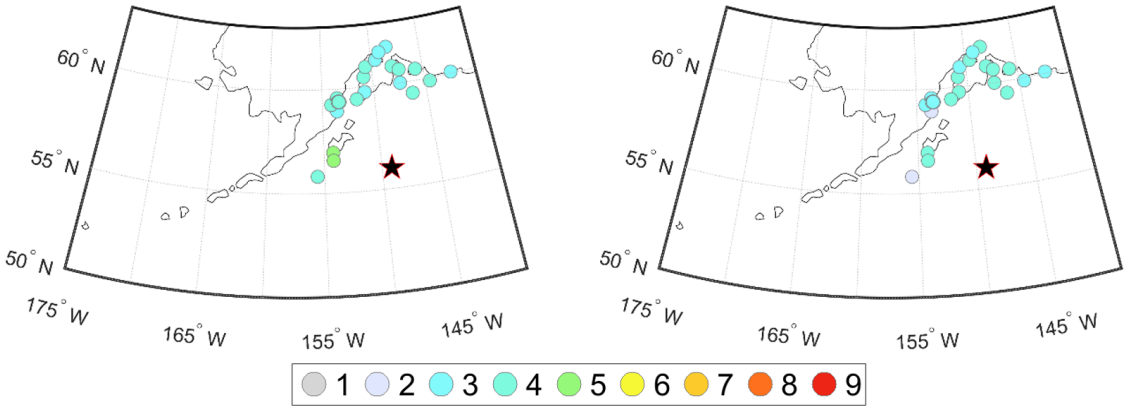

Figure 8. Alaska regionally modeled (left) and DYFI reported (right) macro-intensity values during M_W 7.9 - 280 km SE of Kodiak earthquake.

If we apply the global model to the M_W 7.8 - 99 km SSE of the Perryville earthquake (Figure 9), we can see that the intensities of earthquakes can be significantly underestimated.

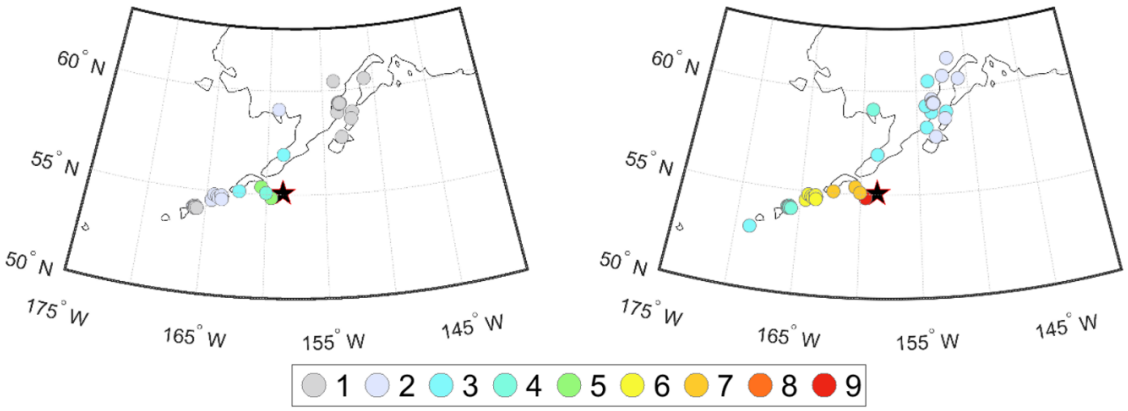

Figure 9. Globally modeled (left) and DYFI reported (right) macro-intensity values during M_W 7.8 - 99 km SSE of Perryville (Alaska) earthquake.

5. Conclusions

We used high-rate GNSS data provided by UNAVCO and New Zealand GeoNet from 6 selected earthquakes from the years 2016-2020. The selection of suitable candidates for PPP processing was performed based on the quality control results from G-Nut/Anubis, when data completeness were considered. In total, data from 182 GNSS stations were processed when utilizing the PPP method. We compared results from two estimation strategies: 1) using the forward square root filter (FLT) and 2) combination the forward filter and the backward smoothing (SMT). We conclude that the SMT solution improved the accuracy of estimated receivers' coordinates and was thus better for further analyses.

Peak ground displacements (PGD) extracted from coordinates time series at individual GNSS sites were used to estimate earthquake magnitude. Moment magnitude estimates calculated as the mean of the magnitudes at each site were compared to the USGS reference values. SMT solution showed the 20% improvement in the accuracy of the moment magnitude estimate compared to the FLT solution (mean of $RMS_{SMT} = 0.18$, mean of $RMS_{FLT} = 0.22$). The mean differences between the USGS moment magnitude reference values and our solution were 0.07 M_W for SMT and 0.09 M_W for FLT.

The Intensity-PGD model calculated on the basis of our analyses of GNSS observations collected at stations surrounding the six globally distributed earthquakes and the model based on PGDs from the Database of Strong-Motion Displacements [7] reached a very good agreement. However, we can see more significant differences in model coefficients between the global and regional (Alaska) models. Therefore, the global model is not optimal for regional applications. Such regional dependency was also observed when comparing our intensity-PGD models with the data provided by the DYFI service. When we applied the estimated regional model coefficients, the achieved intensity was much more consistent with the DYFI data compared to the case when we used the global model. As a results, earthquake intensity can be estimated on the basis of GNSS observations with comparable accuracy that data provided by the DYFI service. The most important advantage of the GNSS analyses is fast objective results applicable in warning systems, which would be very useful for targeting rescue services to the areas affected by an earthquake.

Acknowledgment

This paper was supported by faculty research project FAST-J-21-7178 of the internal grant system BUT. The authors gratefully acknowledge the UNAVCO and the New Zealand GeoNet for providing high-rate GNSS data. We also thank the CODE for release the latest CODE repro3 satellite orbits and clocks.

References

[1] T. Hanks and H. Kanamori, "A moment magnitude scale", Journal of Geophysical Research, vol. 84, no. B5, pp. 2348-2350, 1979. doi:10.1029/jb084ib05p02348
[2] L. Ottemoller and J. Havskov, "Moment Magnitude Determination for Local and Regional Earthquakes Based on Source Spectra", Bulletin of the Seismological Society of America, vol. 93, no. 1, pp. 203-214, 2003. doi:10.1785/0120010220
[3] J. Shuanggen and Z. Wenyao, "Active Motion of Tectonic Blocks in East Asia: Evidence from GPS Measurement", Acta Geologica Sinica - English Edition, vol. 77, no. 1, pp. 59-63, 2003.
[4] G. Blewitt, C. Kreemer, W. C. Hammond, H. -P. Plag, S. Stein, and E. Okal, "Rapid determination of earthquake magnitude using GPS for tsunami warning systems", Geophysical Research Letters, vol. 33, no. 11, 2006. doi: 10.1029/2006GL026145
[5] B. Gutenberg, "Amplitudes of surface waves and magnitudes of shallow earthquakes", Bulletin of the Seismological Society of America, vol. 35, no. 1, pp. 3–12, 1945.
[6] B. W. Crowell, D. Melgar, Y. Bock, J. S. Haase, and J. Geng, "Earthquake magnitude scaling using seismogeodetic data", Geophysical Research Letters, vol. 40, no. 23, pp. 6089-6094, 2013. doi:10.1002/2013GL058391
[7] C. J. Ruhl, D. Melgar, J. Geng, D. E. Goldberg, B. W. Crowell, R. M. Allen, Y. Bock, S. Barrientos, S. Riquelme, J. C. Baez, E. Cabral-Cano, X. Pérez-Campos, E. M. Hill, M. Protti, A. Ganas, M. Ruiz, P. Mothes, P. Jarrín, J. -M. Nocquet, J. -P. Avouac, and E. D'Anastasio, "A Global Database of Strong-Motion Displacement GNSS Recordings and an Example Application to PGD Scaling", Seismological Research Letters, vol. 90, no. 1, pp. 271-279, 2018. doi: 10.1785/0220180177
[8] S. Jin and K. Su, "Co-seismic displacement and waveforms of the 2018 Alaska earthquake from high-rate GPS PPP velocity estimation", Journal of Geodesy, vol. 93, no. 9, pp. 1559-1569, 2019. doi:10.1007/s00190-019-01269-3
[9] K. Su and S. Jin, "Real-Time Seismic Waveforms Estimation of the 2019 MW = 6.4 and Mw = 7.1 California Earthquakes With High-Rate Multi-GNSS Observations", IEEE Access, vol. 8, pp. 85411-85420, 2020. doi: 10.1109/ACCESS.2020.2992193
[10] Z. Hongcai, D. Melgar, and D. E. Goldberg, "Magnitude Calculation without Saturation from Strong-Motion Waveforms", Bulletin of the Seismological Society of America, vol. 111, no. 1, pp. 50-60, 2020. doi:10.1785/0120200133
[11] H. O. Wood and F. Neumann, "Modified Mercalli intensity scale of 1931", Bulletin of the Seismological Society of America, vol. 21, no. 4, pp. 277-283, 1931.
[12] U.S. Geological Survey, "Did You Feel It? Earthquake Observation Reporting", U.S. Geological Survey, 2017. doi: 10.5066/F7J101C8
[13] I. Selmke, R. Dach, D. Arnold, L. Prange, S. Schaer, D. Sidorov, P. Stebler, A. Villiger, A. Jaeggi, and U. Hugentobler, "CODE repro3 product series for the IGS", Astronomical Institute, University of Bern, 2020. doi: 10.7892/boris.135946
[14] U.S. Geological Survey, "Earthquake Lists, Maps, and Statistics", U.S. Geological Survey, 2021. Accessed June 8, 2021 at URL https://www.usgs.gov/natural-hazards/earthquake-hazards/lists-maps-and-statistics
[15] P. Vaclavovic and J. Dousa, "G-Nut/Anubis: Open-Source Tool for Multi-GNSS Data Monitoring with a Multipath Detection for New Signals, Frequencies and Constellations", in IAG 150 Years, Cham: Springer International Publishing, 2016, pp. 775-782. doi: 10.1007/1345_2015_97
[16] P. Václavovic and O. Nesvadba, "Comparison and assessment of float, fixed, and smoothed precise point positioning", Acta Geodynamica et Geomaterialia, pp. 329-340. doi: 10.13168/AGG.2020.0024
[17] C. B. Worden, M. C. Gerstenberger, D. A. Rhoades, and D. J. Wald, "Probabilistic Relationships between Ground-Motion Parameters and Modified Mercalli Intensity in California", Bulletin of the Seismological Society of America, vol. 102, no. 1, pp. 204-221, Feb. 2012.